small NANO MICRO

Biomolecular motors

DOI: 10.1002/smll.200500153

Efficient Designs for Powering Microscale Devices with Nanoscale Biomolecular Motors

*Chih-Ting Lin, Ming-Tse Kao, Katsuo Kurabayashi, and Edgar Meyhöfer**

***C**urrent MEMS and microfluidic designs require external power sources and actuators, which principally limit such technology. To overcome these limitations, we have developed a number of microfluidic systems into which we can seamlessly integrate a biomolecular motor, kinesin, that transports microtubules by extracting chemical energy from its aqueous working environment. Here we establish that our microfabricated structures, the self-assembly of the bio-derived transducer, and guided, unidirectional transport of microtubules are ideally suited to create engineered arrays for efficiently powering nano- and microscale devices.*

Keywords:
- bionanotechnology
- kinesin
- microfluidic systems
- molecular motors

1. Introduction

In biological systems, cellular activities such as intercellular mass transport, cell division, and various forms of cell motility and contractility are all driven by biomolecular motors. Among various biomolecular motors, conventional kinesin (now referred to as kinesin-1) holds significant potential for nanotechnology applications because it is compact (the actual motor domains are <10 nm), efficient ($\approx 50\,\%$), moves robustly in vitro, and extracts chemical energy from its aqueous working environment.[1] Kinesin generates linear, stepwise motion along microtubules (a filamentous cytoskeletal polymer) toward their plus-end by alternately advancing its two motor domains in a hand-over-hand manner.[2] Each of the resulting 8-nm steps is coupled to the binding and hydrolysis of one molecule of adenosine triphosphate (ATP).[3]

Of particular significance for future nanotechnology applications of biomolecular motors are strategies to effectively interface with and extract sufficient mechanical power from this nanometer-scale machine. However, the force generated by a single kinesin molecule is miniscule ($\approx$5–6 pN)[4] and needs to be scaled up to drive manmade microstructures. In nature, cells generate large forces and substantial mechanical power by utilizing highly ordered arrays of motor proteins. For example, in skeletal muscle cells myosin motors and actin filaments are precisely aligned in the nearly crystalline structure of the sarcomere to harness the collective forces (up to 100 N) and motion (up to $10\,\mathrm{m\,s^{-1}}$) from a very large number ($>10^{13}$) of individual motor molecules. We need to follow nature's strategy and develop new technology to selectively pattern and functionally integrate kinesin molecules and microtubules into engineered microstructures. As the direction of motion of kinesin motors along microtubules is determined by the structure (polarity) of the microtubule and directed towards its plus-end, the most critical and challenging requirement is to unidirectionally guide, sort, and align microtubules such that they can serve simultaneously for many motors as nanoscale tracks. Accordingly, micrometer-scale structures may be driven by kinesins along such aligned microtubule tracks to generate meaningful motion and mechanical power.

Simple physical confinement of gliding microtubules by sidewalls has been demonstrated[5] using a linear microchannel patterned on a kinesin-coated glass substrate. Unfortunately, the guided motion in this earlier work was not unidirectional, and gliding microtubules frequently detached from the channel tracks. To achieve unidirectional micro-

[*] Prof. K. Kurabayashi, Prof. E. Meyhöfer
Department of Mechanical Engineering, University of Michigan
2350 Hayward Street, Ann Arbor, MI 48109 (USA)
Fax: (+1) 734-615-6647
E-mail: meyhofer@umich.edu
C.-T. Lin
Department of Electrical Engineering and Computer Science
University of Michigan (USA)
M.-T. Kao
Department of Biomedical Engineering
University of Michigan (USA)

tubule sorting, Hiratsuka[6] introduced arrow-shaped structures into their microchannels and used experimental conditions to selectively adsorb motor proteins into the channels. This approach demonstrated that it was feasible to arrange microtubules by using a proper structural design, however, the design still suffered from frequent detachment of microtubules and unsatisfactory sorting performance. For instance, only about 70% of total microtubules were guided in the proper direction. To address some of these limitations, another group[7] introduced channel overhangs to reduce microtubule loss, but this technique makes it impossible for any other (microfabricated) structures to engage with the microtubules for power extraction. Yet another group[8] used an external flow field to obtain unidirectional microtubule movement. While improved microtubule alignment was achieved, the method is not suitable for microscale fluidic systems or arrays because the large scale of the required external flow does not permit local control of microtubule movement. In addition, previous studies usually relied on photoresist as the structural material for the microfluidic channels; alternative materials would be more desirable as photoresist rapidly swells in an aqueous environment.

The long-term goal of our work is to develop autonomous nano- to microscale transport systems that extract power from kinesin molecules and translocate microfabricated shuttle structures with molecular precision along defined pathways of complex microfluidic systems (see Figure 1). To extract collective force and mechanical power from a group of kinesin molecules moving on microtubule tracks, the microfluidic channel design needs to allow for a) efficient collection and retention (self-assembly) of microtubules, b) satisfactory unidirectional microtubule sorting, c) physical access to external micromechanical device structures or components, and d) stability in aqueous environments. In this paper we present a new microfluidic channel design that meets these requirements as shown in Figure 1A, and on the basis of quantitative experimental observations we develop a mechanistic understanding of the guided sorting and assembly of microtubule tracks in our devices.

2. Results and Discussion

We used three different circular microfluidic channel designs (Figure 2) to study the influence of channel shape and geometry on the sorting performance. Each of the designs consists of a circular channel with a width of a few micrometers (5 μm for Design 1 and Design 2; 6 μm for Design 3) with differently shaped motion rectifiers, which are sup-

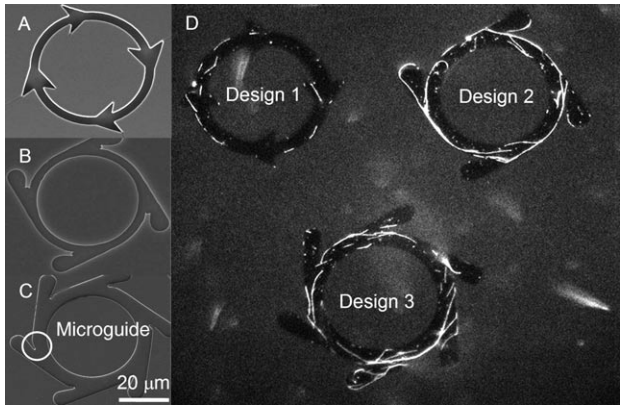

Figure 2. SEM images of the channels in A) Design 1, B) Design 2, and C) Design 3. The microguide structure of Design 3 can be clearly shown in (C). D) Fluorescence microscopy image of the microfluidic-channel designs operated under identical conditions in a single device structure. All three designs support unidirectional motility of sorted microtubules, but under identical conditions Designs 2 and 3 contain more microtubules than Design 1.

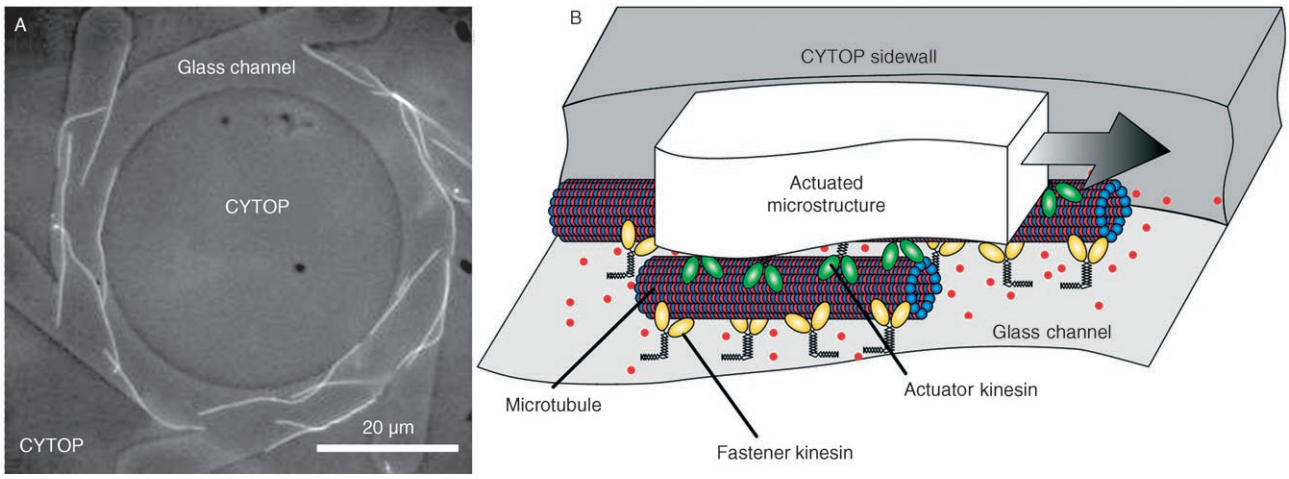

Figure 1. A) Optical image of a microfluidic channel design for effective unidirectional sorting of microtubules. A fluorocarbon polymer (CYTOP) pattern forming the channel sidewalls achieves selective microtubule motility. B) Design concept for powering microscale structures with nanoscale biomolecular motors. The fastener kinesin (yellow) is first used to align microtubules in the microfluidic channels, subsequently it is exploited to permanently immobilize, via a chemical crosslink, aligned microtubules (blue) onto the microfliuidic channel surface. The actuator kinesin (green) drives the transport of manmade microstructures by hydrolyzing ATP (red dots) from the microfludic environment requiring no external power source.

NANO MICRO small

posed to change the direction of the motion of microtubules such that all microtubules in a channel rotate in the same direction.

Design 1 has four motion rectifiers with a sharp arrowhead shape. Experimental observations of the poor turning and detachment behavior of microtubules in the sharp corners of the arrow heads and theoretical predictions of the guiding of microtubules in microchannels on the basis of a statistical mechanics model (described below) motivated Designs 2 and 3 with rounded rectifier corners to reduce the bending energy of microtubules following channel sidewalls. Design 3 has two additional rectifiers and a microstructural feature (see Figures 2 and 3), which we call a "microguide", to influence the distribution of microtubules within the microchannel. Figure 2D shows a fluorescence microscopy image of the three microchannel designs and labeled microtubules during self-assembly and directional sorting. Long image sequences of such events were used to characterize the functional properties of the different designs. All three microchannel designs support motility and upon sorting microtubules move, as expected, clockwise in Design 1 and counterclockwise in Designs 2 and 3.

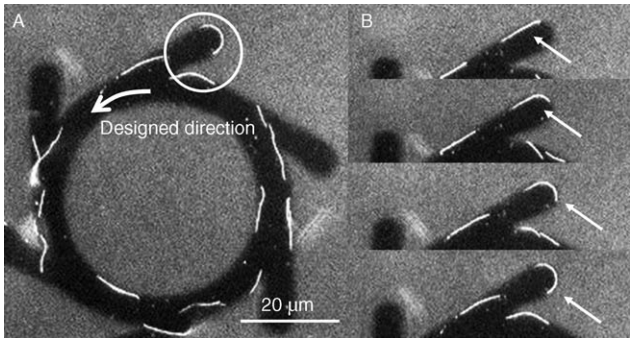

Figure 3. Turning of a microtubule to the designed direction in a rectifier. A) Optical image of the channel of Design 3. B) Image sequence of a microtubule redirected in the rectifier pattern.

The total number of microtubules assembled in a channel at steady state is determined by the equilibrium between the rates of landing in and detaching from the channel. The high concentration of microtubules in the motility buffer and the large buffer volume ensure that the free microtubule concentration remains unaffected during our observations. It is therefore reasonable to assume that the landing rate of microtubules, k (the number of microtubules landing and moving inside the entire channel surface per unit time, number per minute), stays constant throughout the sorting process.

Following this assumption, the governing equation for the total number of microtubules as a function of time, $N_{MT}(t)$, is given by

$$\frac{dN_{MT}(t)}{dt} = k - pN_{MT}(t) \quad (1)$$

where p (min^{-1}) is the microtubule detachment probability per unit time. The solution to Eq. (1) is

$$N_{MT}(t) = \frac{k}{p}[1 - \exp(-pt)] \quad (2)$$

Obtaining the two rates k and p from experimental data allows us to quantitatively assess the performance of each channel design. Figure 4 shows how the number of the microtubules collected in the channel and the fitted theoretical curves change as a function of time for each design. For reference, the same measurements were performed for an unprocessed bare cover-glass surface. We included only microtubules longer than 1.5 μm in length in this analysis to avoid double counting, as some of the shorter microtubules are fragments detached from much longer microtubules moving in the microfluidic channel.

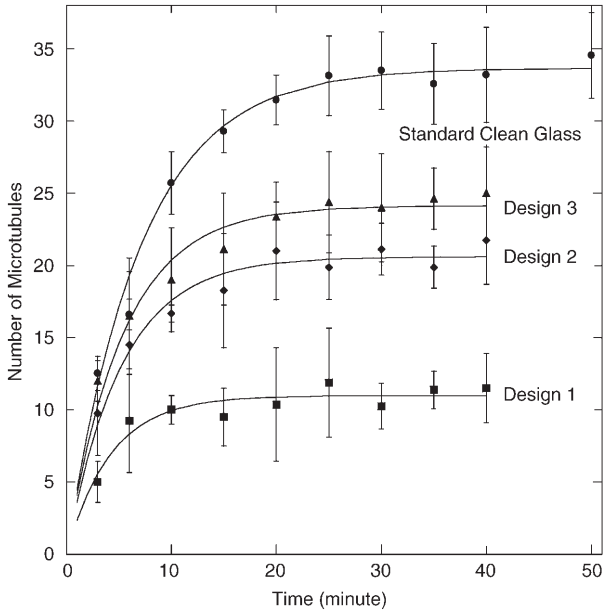

Figure 4. Total number of microtubules gliding within the different microchannel designs as a function of time during the sorting process. The dashed lines show theoretical curves obtained from Eq. (2) with the key parameters fitted to the experimental data.

The experimentally measured landing and detachment rates for each design are summarized in Table 1. The larger initial slopes of the curves for Designs 2 and 3 are consistent with their higher microtubule landing rates. The larger landing rate and lower detachment probability of Designs 2 and 3 explain the larger number of collected microtubules at steady state.

To understand the detailed mechanisms responsible for the above results, we divide our microchannel structures into a rectifier region and a circular channel region, as illustrated in Figure 5. Figure 6A compares the microtubule landing events measured for these regions. It is clear that landing events occur more frequently in the rectifier region. Figure 6B shows a particular microtubule landing event at the wider channel area near the Y-shaped junction between the rectifier pattern and circular channel of Design 3. We repeatedly observed that landing primarily occurred in this part of the channel. Also, the wider channel cross section of

Table 1. Landing (microtubules per minute) and detachment rates (per minute per channel) measured for more than 160 samples of the various channel designs and cover-glass surfaces. Landing and detachment rates on flat, geometrically unconstrained cover glasses are expected to represent (optimal) reference rates. Parameters for the cover glass were normalized to an equivalent surface area as compared to the microfluidic channel designs.

	Design 1	Design 2	Design 3	Cover glass
Landing rate k	2.601 ± 0.378	3.948 ± 0.333	4.483 ± 0.376	4.787 ± 0.155
Detachment rate p	0.237 ± 0.038	0.1916 ± 0.0180	0.1858 ± 0.0180	0.1422 ± 0.005
Difference of the landing rate k compared to cover glass	-2.186	-0.839	-0.304	–
Difference of the detachment rate p compared to cover glass	0.0813	0.0345	0.0348	–

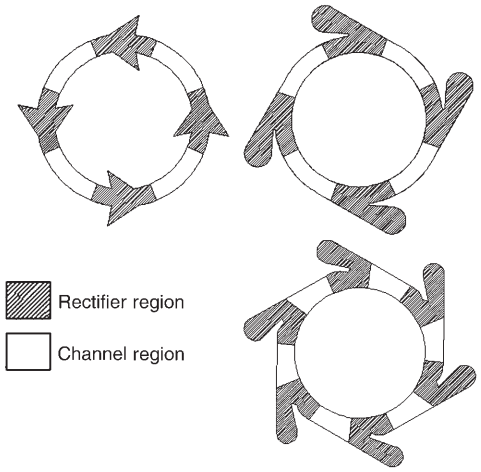

Figure 5. Rectifier and channel regions as defined by the angular symmetric configuration of the different designs.

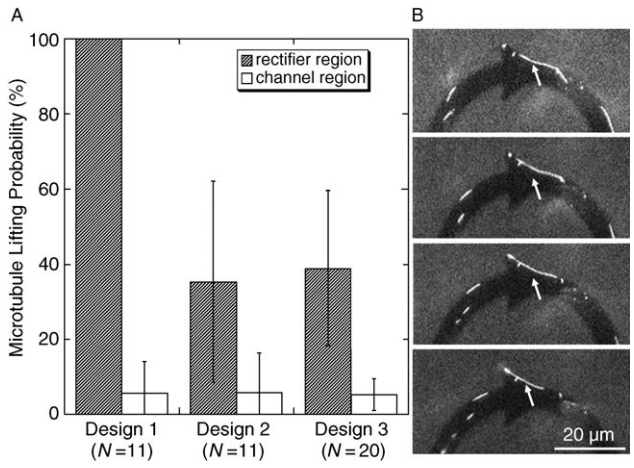

Figure 6. A) Experimental data showing the distribution of landing events in the channel and rectifier regions of the different channel designs. The wider local channel areas of Designs 2 and 3 result in a higher landing ratio. Design 1 does not have any locally wider channel area. B) Microtubule landing sequence near the rectifier pattern of the Design 3 channel.

Designs 2 and 3 in the rectifier portion is responsible for the higher landing rate of these designs. This can be understood by calculating the probability of a microtubule landing and moving in the different microchannel designs. Assuming that microtubules behave as rigid rods (a reasonable assumption as the persistence length of a microtubule is several millimeters) randomly diffusing into the channel from solution and moving upon contact with the kinesin-coated floor (but not the CYTOP sidewalls), a wider channel provides more incident directions for a microtubule with less geometric constraint, leading to a higher local landing probability. Our simple calculations predict, in agreement with the experimental observations, that the landing rate in the rectifier region of Design 2 is about double that of Design 1. As Design 3 offers the least geometrical constraints for microtubules to diffuse into this microchannel, we predict landing rates that are about 1.5 times higher than those of Design 2.

In addition to the landing rate, the number of microtubules in our microfluidic devices is decisively influenced by the detachment or lift-off of microtubules. Figure 7A summarizes our experimental observations on microtubule detachment events observed in the rectifier and circular channel regions of the three designs. Clearly, lift-off events most frequently occur in the rectifier region and are directly related to the mechanical guiding of the microtubule by the channel sidewall. To quantitatively understand the detachment of microtubules from the microfluidic channel, a (statistical mechanics) model was developed that computes the probability of microtubule detachment.

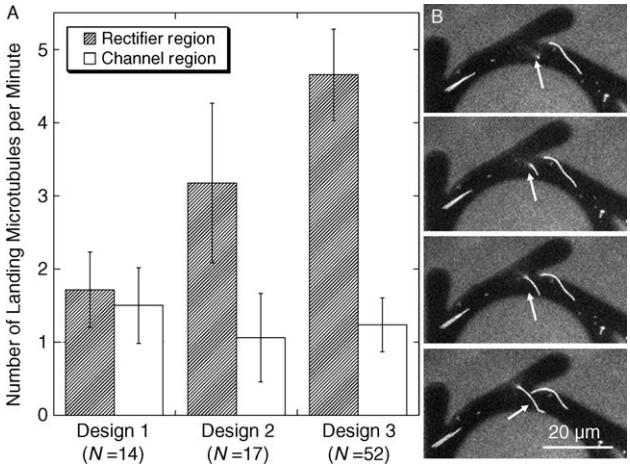

Figure 7. A) Experimental data showing the microtubule detachment probability in two channel regions for various channel designs. The probability was calculated from detaching microtubules and the total number of microtubules in a specific region. The majority of the detachment events occurred in the rectifier region because of the large bending energy required for the microtubule to turn in these regions. It should be noted that the detachment probability of the Design 1 rectifier region is 100%, because an extremely large bending energy is needed to guide microtubules along this structure. B) Microtubule detachment sequence at the sharp edge of the rectifier pattern of the Design 1 channel.

NANO MICRO small

During normal gliding on the bottom surface of the microfluidic channels, microtubules are prevented from detaching by kinesins that maintain continuous physical contact with the microtubules as they are pushed forward. When microtubules encounter a sidewall during the gliding process they are mechanically redirected and locally bent to accept the shape (bending angle θ) of the sidewalls. The energy for this process is provided by the cumulative action of many kinesin molecules leading to potentially large mechanical bending energy storage in the microtubule. In our model detachment will occur if the bending energy of the microtubule exceeds the binding energy of the kinesin–microtubule complex. We presume that microtubules are elastic rods guided by channel sidewalls with a perfectly smooth surface. When bending occurs, each microtubule stores energy given by:[9]

$$U = \frac{EI}{2L}\theta^2 \tag{3}$$

where E is the Young's modulus of the microtubule, I is the moment of inertia of the microtubule, L is the length of the microtubule, and θ is the bending angle determined by the local channel curvature. Assuming a flexural rigidity of $1.9\times10^{-24}\,\mathrm{N\,m^2}$,[10] an average spacing of functional kinesins of 100 nm, and a kinesin–microtubule binding energy of half of the free energy of ATP hydrolysis ($\approx 50\times10^{-21}$ J), our calculations predict microtubule bending energies of 1.05×10^{-17} J, 9.26×10^{-20} J, and 8.42×10^{-21} J for a microtubule following the rectifier of Design 1, the rectifier of Designs 2 and 3, and the circular channel region, respectively. Because of the sharp turning angle in the rectifier of Design 1, the bending energy for a microtubule to follow the sharp channel shape is much larger than for the other designs, and it is also much larger than the energy available from the hydrolysis of ATP during the stepwise motion of kinesin. We expect that the large bending energies in the microtubules could be generated by the concerted action of many kinesins, but during the mechanical interaction of the microtubule with the CYTOP sidewall, this large bending energy inevitably leads to an upward directed-force component. This detaches the microtubule from kinesins at its leading end, because the bending energy of the microtubule is much larger than the maximum binding energy available from a single kinesin–microtubule interaction, thus resulting in the extremely high lifting probability in the arrow-shaped region. Consequently, the model predicts that microtubules will not be able to turn in the sharp corner of the Design 1 rectifier, there is a small, but significant detachment probability in the round rectifier of Designs 2 and 3, and a very low detachment probability when a microtubule follows the channel region of the tested devices. These predictions are in good agreement with our experimental data (Figure 7, Table 1), which suggests that our model is well suited to predict the microtubule detachment behavior and should be used to guide design improvements of future devices.

Next, we have studied how many microtubules among those captured are unidirectionally sorted in these channels. Figure 8 shows the number of microtubules gliding in the designed direction and the ratio of sorted microtubules as functions of time for each design. This process reaches a steady state after about 25 min, and achieves a sorting ratio slightly above 90% regardless of the design. While there is no obvious difference in the time variation of the sorting ratio among the designs, the largest number of sorted microtubules is always achieved in the same amount of time by Design 3. At steady state, both the landing and detachment of microtubules continues to occur while the total number of microtubules in the microfluidic channel remains constant. Some of the (previously) sorted microtubules escape from the channel while new microtubules from solution land in the channel, of which initially one half glide in the reverse direction. As a result, the steady-state sorting ratio never reaches 100%. In a control experiment we removed the free microtubules by washing with a buffer solution without microtubules and repeated the above experiment (Design 3). Under these conditions sorting ratios of $>98\%$ were measured, consistent with our previous conclusions.

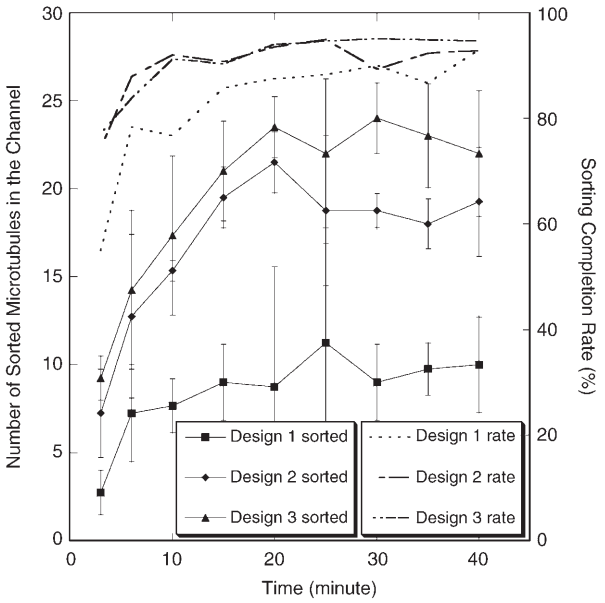

Figure 8. Time dependence of the total number of sorted microtubules and sorting ratio for various channel designs. All of the channel designs achieve a 90% sorting ratio after 25 min. The actual number of the sorted microtubules for Design 1 is much smaller than those for Designs 2 and 3.

Finally, we have examined the spatial distribution of the sorted microtubules across the channel for each design. The gliding microtubules tend to approach the outer channel sidewall. This can also be explained by considering the bending energy state of the gliding microtubules. The gliding along the outer channel sidewall results in a minimum bending curvature, thus providing the lowest-energy path for the microtubules. However, our future goal is to extract mechanical power from sorted microtubules. This requires the microtubules to engage with other external microscale mechanical components. For this purpose, a design leading to a uniform cross-channel microtubule distribution is highly desirable. To redirect the microtubules away from the outer channel sidewall, we introduced the microguide

structure as shown in Figure 9A and B to channel Design 3. Due to its inwards-oriented curved shape, this structure redirects gliding microtubules towards the inner channel sidewall (Figure 9C). Figure 10 shows the cross-channel spatial distribution of microtubules at various times. It clearly shows that the distribution remains fairly uniform in Design 3 while the two other designs exhibit a larger number of microtubules near the outer channel sidewall as time increases. This result indicates a significant impact of the microguide structures on the resulting cross-channel microtubule distribution.

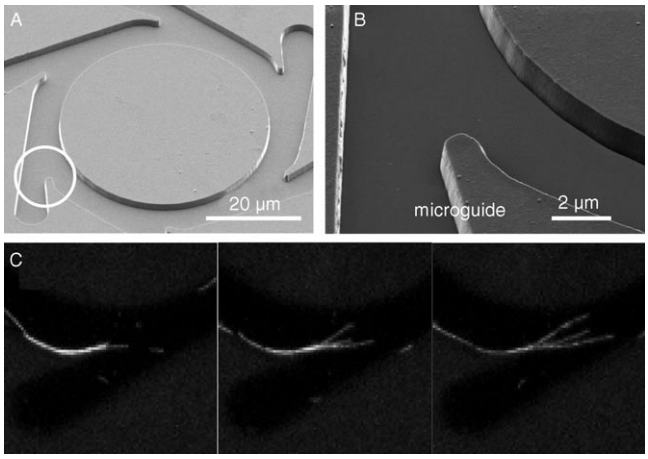

Figure 9. A) SEM images of a microfluidic channel in Design 3. B) Microguide structure in the channel of a Design 3 device. C) Sequential optical images illustrate the redistribution of microtubules within the microchannel by the microguide.

3. Conclusion

In summary, we have designed, fabricated, experimentally tested, and modeled microtubule unidirectional sorting mechanisms that make possible efficient integration of nanoscale biomolecular motors and microengineered device structures. Future devices based on the findings presented here will be suitable for powering MEMS and microfluidic devices without external power sources at unprecedented low-power levels. We are currently exploring implementations for sorting molecules and extracting mechanical power for the actuation of microscale mechanical devices and fluids.

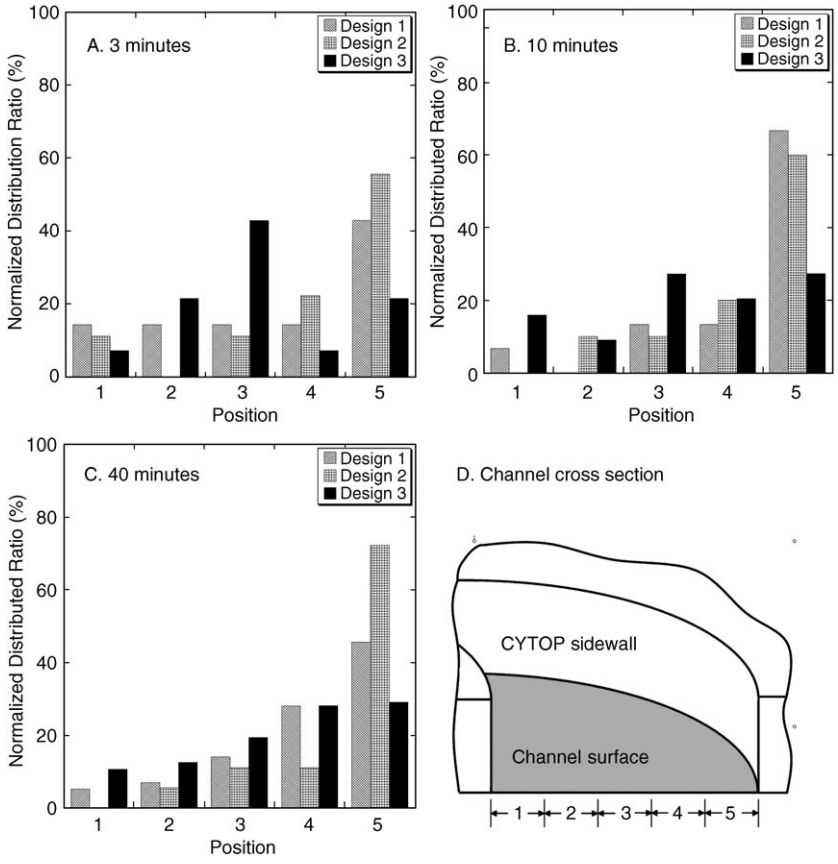

Figure 10. Microtubule positional distribution across the channel for each design after A) 3 min, B) 10 min, and C) 20 min. D) Schematic view of a microfluidic channel cross section. The position coordinate is taken across the channel from the inner side to the outer side. The origin is located at the edge of the inner channel sidewall. Initially, the microtubules are relatively uniformly distributed across the channel due to the randomness of the landing process. After the sorting process, a majority of the microtubules are located close to the outer sidewall in Designs 1 and 2. The microguide structure helps microtubules to stay more uniformly distributed across the channel of Design 3.

4. Experimental Section

The microchannels utilized for our work consist of a circular pattern etched into a layer of fluorocarbon polymer, CYTOP,[11] deposited on a glass substrate. The thickness of the CYTOP layer is typically 1.5 μm. Previous work[12] indicates that the CYTOP coating suppresses nonspecific protein binding. We have found a very large contrast between the numbers of gliding microtubules on bare and CYTOP-coated glass surfaces in a gliding assay. We believe that this differential in motility is due to the selective adsorption or selective functionality of kinesin on the exposed glass surface of the channel bottom. To fabricate these channels, we first prepared a cover-glass substrate using piranha solution cleaning and diluted HF (1:20) surface treatment. A CYTOP film was spun on the cleaned glass substrate at 1500 rpm followed by a 30-min curing step at 180 °C in an oven. Following standard photoresist lithography, we patterned the channels in the CYTOP film by plasma etching using SF_6 gas at a 20 mTorr pressure, an rf etching power of 120 W, and a gas flow rate of 20 sccm (standard cubic centimeters per minute). Finally, the cover-glass substrate with the microchannel patterns was treated with NH_4OH:H_2O_2 (1:1) for 5 min. These fabrications reproducibly yield channels with sur-

face properties that allow kinesin binding and microtubule affinity and motility similar to those of control experiments on an unprocessed glass surface. Furthermore, the walls of the microfabricated channels processed in this manner are steep enough to prevent rapid loss (detachment) of microtubules from the microfluidic channels.

For our experiments we used a bacterially expressed kinesin motor, NKHK560cys. This motor consists of the head and neck domain of *Neurospara crassa* kinesin (amino acids 1–433) and the stalk of *Homo sapiens* kinesin (residues 430 to 560) and a reactive cysteine at the C-terminal end.[13] The NKHK560cys gene was ligated into the pT77 plasmid and expressed in *E. coli* BL21 cells using TPM medium with 50 μM ampicillin at 37 °C. Expression was induced by adding 0.1 mM IPTG at a cell density corresponding to an optical density of 0.6–0.8 and continued overnight at 22 °C. Cells were centrifuged and resuspended in lysis buffer containing protease inhibitors, DNAse, and lysozyme, followed by sonification. The supernatant of this was loaded on a SPFF ion exchanger[14] and kinesin was eluted by a step gradient to protocol. Tubulin and TMR-labeled tubulin were obtained by standard procedures.[15] Briefly, tubulin was purified from cow brain by three cycles of microtubule polymerization and depolymerization followed by phosphocellulose ion-exchange chromatography to eliminate microtubule associate protein. Tubulin was labeled with TMR[16] by reacting polymerized microtubules with a 20-fold excess of dye at room temperature for 30 min. Competent, labeled tubulin was purified from this mixture by repeated depolymerization and polymerization. For experiments, microtubules were polymerized by incubating 2 mg mL^{-1} tubulin (equal ratios of TMR-labeled and unlabeled tubulin) 1 mM GTP, and 4 mM $MgCl_2$ in BRB80 buffer at 37 °C for 20 min. Microtubules were stabilized by the addition of 10 μM taxol. Flow chambers were constructed from microscope slides and microfabricated cover glasses containing the microfluidic channels separated by 75-μm-thick glass spacers. Where indicated, flow chambers were first pretreated with 100 μL of a 2 mg mL^{-1} aqueous solution of Pluronic[17] and then washed with 200 μL of deionized water followed by 100 μL of BRB80 buffer. The protein loading procedure was identical to that for standard kinesin gliding assays: Chambers were loaded with kinesin (47 μg mL^{-1} casein and 1.4 μM kinesin in BRB80 buffer) and incubated for 5 min. Subsequently, microtubules in a BRB80 buffer containing 1 mM ATP and an oxygen scavenger system (4 μg mL^{-1} microtubules, 2 mM $MgCl_2$, 10 mM glucose, 100 μg mL^{-1} glucose oxidase, 80 μg mL^{-1} catalase, 10 mM DTT, and 47 μg mL^{-1} casein) were loaded. Samples were observed with an inverted fluorescence microscope (ZEISS Axiovert 200, 40x/1.3 NA Plan Neofluar objective) and images were recorded with a digital CCD camera (Orca II, Hamamatsu, Japan).

Acknowledgements

This work was supported by DARPA contract N66001-02-C-8039. The authors thank Li-Jing Cheng for suggestions in fabrication and Dr. Stefan Lakämper for help with motor protein preparations.

[1] a) R. D. Vale, B. J. Schnapp, T. S. Reese, M. P. Sheetz, *Cell* **1985**, *40*, 449–454; b) S. T. Brady, *Nature* **1985**, *317*, 73–75.
[2] a) A. Yildiz, M. Tomishige, R. D. Vale, P. R. Selvin, *Science* **2004**, *303*, 676–678; b) C. L. Asbury, A. N. Fehr, S. M. Block, *Science* **2003**, *302*, 2130–2134; c) J. Howard, *Nature* **1997**, *389*, 561–567.
[3] W. Hua, E. C. Young, M. L. Fleming, J. Gelles, *Nature* **1997**, *388*, 390–393.
[4] a) A. J. Hunt, F. Gittes, J. Howard, *Biophys. J.* **1994**, *67*, 766–781; b) K. Svoboda, C. F. Schmidt, B. J. Schnapp, S. M. Block, *Nature* **1993**, *365*, 721–727; c) E. Meyhofer, J. Howard, *Proc. Natl. Acad. Sci. USA* **1995**, *92*, 574–578.
[5] a) L. Limberis, R. J. Stewart, *Nanotechnology* **2000**, *11*, 47–51; b) S. G. Moorjani, L. Jia, T. N. Jackson, W. O. Hancock, *Nano Lett.* **2003**, *3*, 633–637; c) L. Jia, S. G. Moorjani, T. N. Jackson, W. O. Hancock, *Biomed. Microdevices* **2004**, *6*, 67–74.
[6] Y. Hiratsuka, T. Tada, K. Oiwa, T. Kanayama, T. Q. P. Uyeda, *Biophys. J.* **2001**, *81*, 1555–1561.
[7] H. Hess, C. M. Matzke, R. K. Doot, J. Clemmens, G. D. Bachand, B. C. Bunker, V. Vogel, *Nano Lett.* **2003**, *3*, 1651–1655.
[8] R. Yokokawa, S. Takeuchi, T. Kon, M. Nishiura, K. Sutoh, H. Fujita, *Nano Lett.* **2004**, *4*, 11, 2265–2270.
[9] a) J. Clemmens, H. Hess, J. Howard, V. Vogel, *Langmuir* **2003**, *19*, 1738–1744; b) J. Clemmens, H. Hess, R. Lipscomb, Y. Hanein, K. F. Bohringer, C. M. Matzke, G. D. Bachand, B. C. Bunker, V. Vogel, *Langmuir* **2003**, *19*, 10967–10974; c) H. Hess, J. Clemmens, C. M. Matzke, G. D. Bachand, B. C. Bunker, V. Vogel, *Appl. Phys. A* **2002**, *75*, 309–313.
[10] H. Felgner, R. Frank, M. Schliwa, *J. Cell Sci.* **1996**, *109*, 509–516.
[11] Asahi Glass Co., Tokyo, Japan, **2001**.
[12] C. S. Lee, S. H. Lee, S. S. Park, Y. K. Kim, G. K. Kim, *Biosens. Bioelectron.* **2003**, *18*, 437–444.
[13] a) T. Funatsu, Y. Harada, H. Higuchi, M. Tokunaga, K. Saito, R. D. Vale, T. Yanagida, *Biophys. Chem.* **1997**, *68*, 63–72; b) A. Kallipolitou, D. Deluca, U. Majdic, S. Lakamper, R. Cross, E. Meyhofer, L. Moroder, M. Schliwa, G. Woehlke, *EMBO J.* **2001**, *20*, 6226–6235; c) S. Lakamper, A. Kallipolitou, G. Woehlke, M. Schliwa, E. Meyhofer, *Biophys. J.* **2003**, *84*, 1833–1843.
[14] SP Fast Flow, Amersham Biosciences, Piscataway, NJ, USA.
[15] A. A. Hyman, *J. Cell Sci. Suppl.* **1991**, *14*, 145–147.
[16] 5,6-Carboxytetramethylrhodamine, Molecular Probes, Eugene, OR, USA.
[17] Pluronic F108 Prill, BASF, NJ, USA.

Received: May 9, 2005
Revised: September 10, 2005
Published online on December 12, 2005

